Thermally Induced Structural Modification of Silica Nanoparticles Investigated by Raman and Infrared Absorption Spectroscopies

G. Vaccaro,* S. Agnello, G. Buscarino, and F. M. Gelardi

Dipartimento di Scienze Fisiche ed Astronomiche, Universitá di Palermo, Via Archirafi 36,
I-90123 Palermo, Italy

We report an experimental investigation by Raman and infrared (IR) absorption spectroscopies on the structural modifications induced by isochronal thermal treatments on amorphous SiO_2 nanoparticles (*fumed silica*). In particular, three different commercial types of this material, characterized by particle mean diameters of 7, 14, and 40 nm, were subjected to thermal treatments from 100 up to 1000 C. We found that some properties of fumed silica, such as the SiOSi mean bond angle, ring size distribution, and surface adsorbed water content, are drastically different from those of common bulk silica materials and intimately related to the particles' dimension. The SiOSi mean bond angle, probed by the main Raman line peaked at about 440 cm^{-1}, is modified by thermal treatments above 400 C and tends toward typical values of bulk silica materials, whereas the three-membered ring population, probed by the D_2 line peaked at about 600 cm^{-1}, changes but does not reach bulk silica features. The surface adsorbed water content, estimated by IR measurements, gradually decreases, starting from 100 C. The peculiar properties of fumed silica, which suggest a strained atomic network structure, together with the investigation of its modifications induced by thermal treatments, are interpreted in terms of a shell-like model of the constituting particles. In particular, the model assumes that each particle comprises a *surface shell* characterized by a network structure highly strained and a *core shell* with a less strained structure more similar to that of bulk silica. This model, discussed on the basis of our experimental results, suggests that the structural property modifications induced by thermal treatments into the surface shell are related to the dehydroxylation process and to the buildup of particle-to-particle linking (sintering effects), whereas the structural modifications into the core shell arise from the network relaxation activated by thermal treatments.

Introduction

Fumed silica is a nonporous nanometric silica (amorphous SiO_2) material, obtained by reacting silicon tetrachloride in an O_2/H_2 flame. This process generates small primary particles, with diameters from few to tens of nanometers, which tend to form aggregates with a size of 100−500 nm, that could be linked together in chains to form agglomerates.[1] The wide specific surface area up to hundreds of m^2/g is one of the most particular features characterizing fumed silica. This material is employed in numerous applications as in toothpaste, adsorbents, filler for strength reinforcement, and starting materials for optical fibers.[2−4] Besides, the tendency of today's research toward nanotechnology has significantly increased the interest on these nanometer-sized silica materials for their potential applications in a lot of scientific ambits.[5,6] For all these reasons, many theoretical as well as a wide range of experimental studies were carried out on fumed silica by researchers for many years.

From these studies, it emerged that fumed silica is characterized by spectroscopic features drastically different from those of bulk silica. These differences are well evident in Raman and infrared (IR) absorption spectra. These latter, for example, are mainly governed by a broad line, extending from 2500 to 4000 cm^{-1}, assigned to physisorbed water on the primary particle surface and attributed to the particles' hydrophilic character.[7,8] On the other hand, fumed silica Raman spectra show the main broad line characteristic of bulk silica materials but shifted toward frequencies higher than 440 cm^{-1}. Besides, the well-known D_1 and D_2 Raman lines, peaked at 495 and 605 cm^{-1}, respectively, are much more intense as compared with those of bulk silica materials.[9−12] These findings were interpreted in terms of smaller SiOSi mean bond angles and different distributions of the *n*-membered rings (the shortest closed path of connected tetrahedra, where *n* corresponds to the number of constituent tetrahedra) in the fumed silica network. These interpretations are based on the extension from bulk silica to fumed silica of the attribution of the Raman signals in the range of 200−700 cm^{-1} to oxygen atom displacements of the SiOSi group.[13] In particular, the main Raman line at about 440 cm^{-1} (indicated henceforth as the R-line) is assigned to the O-bending motion of *n*-membered rings with $n > 4$, whereas D_1 and D_2 lines are assigned to in-phase symmetric oxygen breathing vibrations of four- and three-membered rings, respectively.[12−14]

Recent experimental studies showed that, by thermally treating fumed silica with 7 nm diameter particles for a long duration time and at high temperatures (up to ∼200 h at 1000 C), its uncommon spectroscopic features are almost fully deleted, suggesting a conversion toward a bulklike structure. These findings were interpreted on the basis of a sintering process between the particles, in which the nanometric nature of the original system was modified in favor of a bulklike structure.[9] In this context, an electron paramagnetic resonance study by Stesmans et al. on an irradiated SiO/fumed silica/SiO_2 sandwich suggested a shell-like structural model of the primary

* To whom correspondence should be addressed. E-mail: gvaccaro@fisica.unipa.it.

TABLE 1: List of the Employed Materials and Abbreviations, Specific Surface Area, and Primary Particle Mean Diameter

commercial name (abbreviation)	specific surface area [m²/g]	particle diameter [nm]
Aerosil 380 (AE380)	380	7
Aerosil 150 (AE150)	150	14
Aerosil OX 50 (AEOX 50)	50	40

particle.[15] In this model, the *surface shell* of each particle has a strained atomic network structure, whereas the *core shell* is characterized by a bulklike silica.[15] Afterward, the same authors suggested that the core of the nanoparticles is probably not fully identical to that of bulk silica.[16] In particular, the core network shows a SiOSi mean bond angle smaller than that of bulk silica. A similar interpretation was proposed earlier by Uchino et al.[11] They suggested that, not only at the surface but also in the interior of fumed silica primary particles, the distribution of the SiOSi bonding is different from that of the bulk silica materials. On this basis, the thermally induced modifications of the spectroscopic properties of fumed silica could also be imputed to ordinary thermal effects, other than to the occurrence of sintering among primary particles.

Despite the intensive studies done on fumed silica, the structural properties and the mechanisms that lead to the bulklike network during thermal treatments are still not fully understood. Besides, the experimental investigations performed until now were focused mainly on one typology of fumed silica (usually particles with a 7 nm diameter). Driven by the goal to shed new light on these questions, we carried out a correlated investigation by Raman and IR spectroscopies to obtain quantitative information on the modifications induced by thermal treatments from 100 up to 1000 C on the structural properties of three different fumed silica materials, characterized by particle diameters of 7, 14, and 40 nm.

Experimental Section

Commercial fumed silica samples were used (Aerosil by Evonik Industries).[17,18] They were synthesized by $SiCl_4$ oxidation in an O_2/H_2 flame at 1100−1400 C. As-received fumed silica powders were pressed in a uniaxial press at ∼0.3 GPa, forming a cylindric self-supporting powder tablet from which rectangular shaped samples with a size of 5 × 5 × 2 mm³ were obtained and used in all the following reported measurements. In Table 1, the commercial name and abbreviation, specific surface area, and primary particle mean diameter are specified for each of the considered fumed silica materials.

Thermal treatments were carried out in air for 2 h in the range of 100−1000 C, with step of 100 C. The furnace temperature was controlled by a digital system and stabilized within ±3 C. We considered different samples for each fumed silica type, which were thermally treated at different temperatures. In the following, the untreated samples will be referred to as "sample abbreviation/0", whereas the thermally treated ones as "sample abbreviation/T", where T indicates the temperature of the treatment in C units.

Raman measurements were performed at room temperature by a Bruker RAMII Fourier transform Raman spectrometer, employing a 500 mW Nd:YAG laser (1064 nm) source. The spectral resolution was fixed at 5 cm⁻¹. IR spectra were obtained at room temperature with a nitrogen-purged Bruker spectrophotometer (model VERTEX-70) with a spectral resolution of 1 cm⁻¹. To eliminate the effect of residual water in air, the
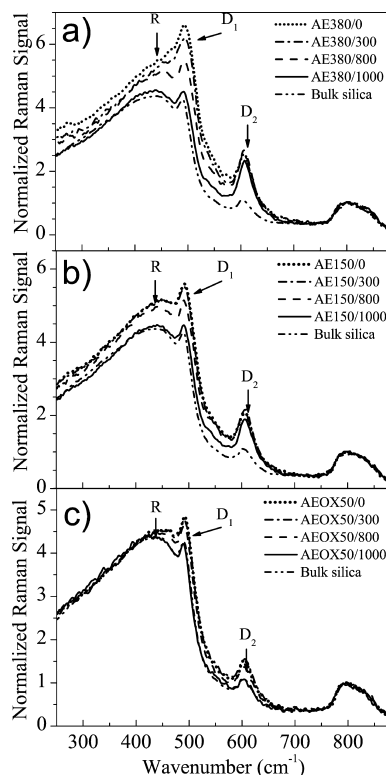

Figure 1. Raman spectra acquired for the materials (a) AE380, (b) AE150, and (c) AEOX50 before and after thermal treatments at 300, 800, and 1000 C. A bulk silica Raman spectrum is reported as a reference. Each spectrum is normalized to the amplitude of the line peaked at ∼800 cm⁻¹. The spectral features evidenced by arrows are discussed in the text.

absorption spectrum of the empty beamline was subtracted from the spectrum of each sample, after suitable normalization.

Results

Figure 1 reports the Raman spectra acquired for (a) AE380, (b) AE150, and (c) AEOX50 samples before and after thermal treatments at 300, 800, and 1000 C. In the same figure, a typical Raman spectrum of bulk silica is reported for comparison. To carry out a quantitative analysis, in agreement with previous studies,[12,19] the spectra were normalized to the amplitude of the line peaked at ∼800 cm⁻¹. This choice is suitable because this line, assigned to the stretching vibration of the SiOSi group, is very stable. For example, it was reported that it does not significantly change by subjecting bulk silica to high hydrostatic pressures, even for pressures that induce permanent densification.[20]

As shown in Figure 1, all the untreated fumed silica samples exhibit a very different Raman spectrum as compared with that of bulk silica: the R-line is more intense and shifted toward higher frequencies, and the D_1 and D_2 lines are more intense. It is worth noting that these properties are much more pronounced on decreasing the primary particles' size. Thermal treatments gradually modify both the R-line and the D_1 and D_2 lines features in different ways. In fact, after the treatment at 1000 C, the R-line of the three fumed silica samples is very similar to that of bulk silica, whereas the amplitude of the D_2 line is still significantly different.

To investigate in a more quantitative way these changes, we estimated the position of the maximum of the R-line (ω_R) as a function of the thermal treatment temperatures. These data are reported in Figure 2. In the same figure, the peak position
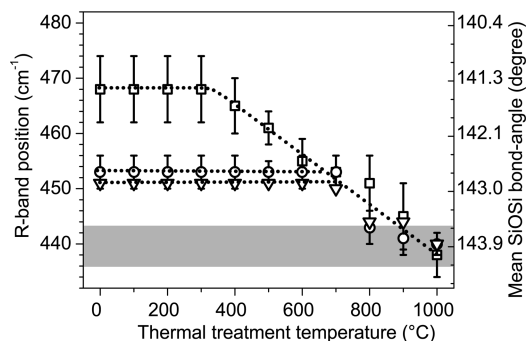
Thermally Induced Structural Modification of Silica NPs

J. Phys. Chem. C, Vol. 114, No. 33, 2010 **13993**

Figure 2. Main Raman line position (ω_R) and the SiOSi mean bond angle (θ), obtained from eq 1, of the materials ($\square$) AE380, ($\bigcirc$) AE150, and (∇) AEOX50 as a function of the thermal treatment temperature. The gray stripe represents the ω_R variability observed in a lot of bulk silica materials of different commercial origins. Dotted lines are guides for the eye.

Figure 3. D_2 line amplitude in the materials ($\square$) AE380, ($\bigcirc$) AE150, and (∇) AEOX50, estimated from the normalized Raman spectra, as a function of the thermal treatment temperature. The gray stripe represents the D_2 line amplitude variability observed in a lot of bulk silica materials of different commercial origins. The inset shows the D_2 line amplitude in the untreated samples as a function of the mean diameter of the primary particles. Dashed or dotted lines are guides for the eye.

variability determined in a wide variety of bulk silica materials of different commercial origins (both natural and synthetic)[21] is also indicated as a gray stripe. As shown in Figure 2, AE150 and AEOX50 materials exhibit the same trend: the ω_R values do not change up to ∼700 °C, whereas they gradually decrease, falling into the gray stripe for $T > 800$ °C. At variance, the R-line position in the AE380 material is constant up to ∼400 °C, and thereafter, it progressively decreases, superimposing for $T \geq 600$ °C to the trend observed for AE150 and AEOX50 materials.

It is worth noting that the R-line position is strongly related to the SiOSi mean bond angle (indicated afterward as the θ angle), whose value can be estimated by the relation

$$\cos(\theta/2) = \frac{\cos(\theta_0/2)}{\omega_0}\omega_R \qquad (1)$$

where $\omega_0 = 437$ cm^{-1} and $\theta_0 = 144$° are reference values.[13] θ values obtained by this equation are reported on the right vertical axis of Figure 2 and suggest that this angle is smaller in fumed silica as compared with the bulk one and that it gradually increases by thermal treatments.

To further compare our Raman spectra, we estimate the amplitude of the D_2 line. A similar study for the D_1 line was not possible because its spectroscopic features are seriously affected by the superposition with the R-line. In particular, to evaluate the D_2 line amplitude in our samples, we subtracted an opportune baseline to the normalized Raman spectra, in agreement with the method of analysis used in previous experimental investigations.[21−23] In the inset of Figure 3, the D_2 line amplitude for the untreated samples as a function of the mean diameter is reported. A linear correlation is clearly evident. In the main panel of Figure 3, we report the D_2 line amplitude as a function of the thermal treatment temperature. In the same figure, we indicate with the gray stripe the amplitude variability of the D_2 line estimated in a wide variety of bulk silica materials of different commercial origins (both natural and synthetic).[21] As shown in Figure 3, fumed silica materials display a very similar trend among them; that is, the D_2 line amplitude does not appreciably change in each material for all thermal treatment temperatures except for the temperatures in the range of 500−800 °C. In this range, the D_2 line amplitude undergoes to detectable variations in all fumed silica materials, reaching a maximum at $T \sim 700$ °C.
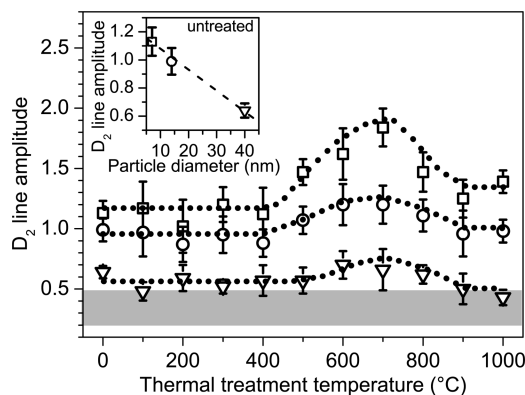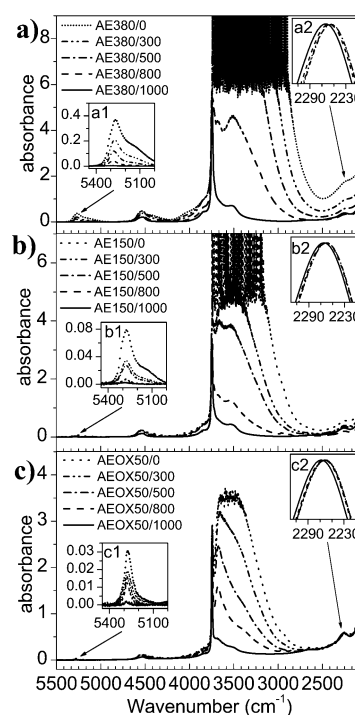

Figure 4. IR spectra acquired for the materials (a) AE380, (b) AE150, and (c) AEOX50 before and after thermal treatments at 300, 500, 800, and 1000 °C. Insets a1, b1, and c1 are zooms of the line around 5200 cm^{-1}, assigned to the combination modes of water molecules ($\nu_1 + \nu_2$ and $\nu_2 + \nu_3$); see the text. Insets a2, b2, and c2 are zooms of the line around 2260 cm^{-1}, subtracted by an opportune baseline and normalized to the maximum, assigned to the overtone of the SiOSi stretching vibration at 1100 cm^{-1}.

In addition to the Raman investigation, the effects of thermal treatments were also explored by IR measurements. The IR spectra of AE380, AE150, and AEOX50 fumed silica materials acquired before and after thermal treatments at 300, 500, 800, and 1000 °C are shown in Figure 4. All the IR spectra of untreated samples show a broad line in the range of 2500−4000 cm^{-1}, whose main contribution arises from the vibrational modes of physisorbed water on the primary particle surface.[7,8] In particular, it was reported that water is multilayer distributed with the first hydration layer hydrogen bonded to surface silanols (isolated, single, geminal, and bridged) and the second layer constituted by water molecules linked together on the same
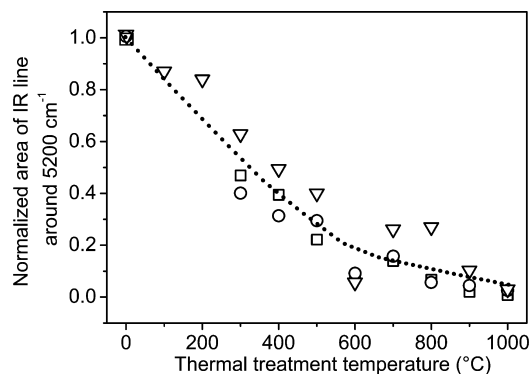
Figure 5. Area of the IR line around 5200 cm^{-1}, normalized to that of untreated samples, for materials (□) AE380, (○) AE150, and (▽) AEOX50 as a function of thermal treatment temperatures. The error bar is comparable to the dimension of the symbols. Dotted lines are guides for the eye.

Figure 6. Peak position of the 2260 cm^{-1}, estimated by a baseline subtraction, in the materials (□) AE380, (○) AE150, and (▽) AEOX50 as a function of the thermal treatment temperatures. The gray stripe represents the peak position variability observed in a lot of bulk silica materials of different commercial origins. The error bar is comparable to the dimension of the symbols. Dotted lines are guides for the eye.

particle and/or linked to water molecules of nearby particles.[7,8,24,25] In agreement with previous work, we also found that the intensity of this line increases on decreasing the primary particles' diameter or, equivalently, on increasing the specific surface area.[7] On the shoulder of this broad line, a narrow line peaked at ∼3740 cm^{-1} can be detected, as clearly evident for AEOX50/0. This line is usually assigned to isolated surface silanols.[25,26]

As shown in Figure 4, the thermal treatments induce a gradual decrease of the broad band in the range of 2500−4000 cm^{-1} in all the samples and reveal the presence of other specific spectral features in the spectra. In detail, two bands at about 3520 and 3680 cm^{-1} are found, suggesting the presence of SiOH groups engaged in H bonding with each other.[27] These bands are also affected by the treatments and decrease on increasing the temperature. Because many IR spectra are saturated in the region of 2500−4000 cm^{-1}, we estimated the water content from absorption bands associated with vibration combination modes in the range of 5000−5400 cm^{-1} (see insets a1, b1, and c1 of Figure 4). These bands are attributed to nearly degenerate $\nu_1 + \nu_2$ and $\nu_2 + \nu_3$ combination modes of bending ($\nu_2 \sim 1630$ cm^{-1}), symmetrical stretching ($\nu_1 \sim 3560$ cm^{-1}), and antisymmetrical stretching ($\nu_3 \sim 3650$ cm^{-1}) modes of water.[8,28] From the insets of Figure 4, it is possible to note that the shapes of these bands depend on the material. In particular, the band profile is more structured on decreasing the particle diameters, suggesting a different contribution of the various vibrational modes. Notwithstanding, we observe that a gradual reduction of the overall band area occurs in all the materials. In Figure 5, we report the area of this band, normalized to that of untreated samples, as a function of the thermal treatment temperatures. The data suggest that the dehydroxylation process is effective in the same temperature range for AE380, AE150, and AEOX50 materials. It is worth noting that the IR spectra have been taken, at worst, within 8 days from the treatment. Because the samples were kept at ambient conditions during this time, rehydration effects could affect our measurements. However, we can state that the thermal treatments are able to remove water starting from 100 C because a decrease of the water associated bands is anyway found.

IR spectra can be used also to investigate some relevant structural features of the materials. In particular, the position of the IR line around 2260 cm^{-1}, assigned to the first overtone of the SiOSi stretching vibration mode, is correlated to the fictive temperature T_f (the high temperature at which silica is allowed to reach thermal equilibrium before the rapid quench to room
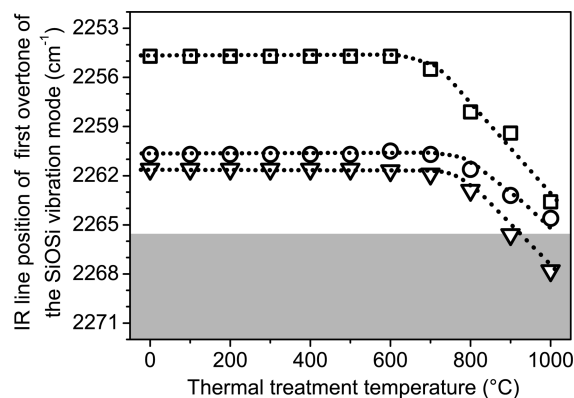
temperature).[29] This latter is relevant because it is related to the average value of the SiOSi bond angle.[30−32] As shown in Figure 4, in many spectra of our samples, one cannot identify a maximum of the line around 2260 cm^{-1} because it is dramatically overlapped to the tail around ∼2100 cm^{-1} (see, for example, AE380/0, AE380/300, and AE150/0 samples). In addition, for those samples in which the maximum can be recognized, it typically falls below 2255 cm^{-1}. These findings prevent directly estimating the fictive temperature from our IR spectra. In fact, the relation linking the peak position and the T_f is only valid in a small frequency range from ∼2255 to ∼2263 cm^{-1} and when the peak is estimated without baseline subtraction.[30−32] Accounting for the above limitations, we limited ourself to obtaining qualitative information on the SiOSi mean bond angle from IR spectra to support results obtained from Raman measurements. To this aim, we analyzed the region around 2260 cm^{-1} by subtracting a linear baseline from the IR spectra. The spectra obtained with this method are reported, normalized to the maximum, in the insets a2, b2, and c2 of Figure 4 and show a line peaked at about 2260 cm^{-1} in all the samples. This line in all the samples has a similar shape independent of the temperature, but the peak position shifts toward higher frequencies on increasing the temperature.

The peak positions obtained from this analysis method for AE380, AE150, and AEOX50 materials are reported in Figure 6. In the same figure, we indicate with the gray stripe the variability obtained for this line in a wide variety of bulk silica materials of different commercial origins, estimated by applying the same analysis method used for the fumed silica samples. Therefore, even if the line position is shifted and it cannot be related to the T_f, the comparison between fumed and bulk samples is still valid and it can give information on the different structural properties of the materials. The data reported in Figure 6 show a trend in qualitative agreement with that of the R-line position reported in Figure 2. In particular, all the fumed silica untreated materials have an IR line peak position different from that of the bulk silica. Furthermore, AE150 and AEOX50 have similar peak positions with each other, which are not modified up to ∼700 C. For higher temperatures, these values monotonically decrease toward the bulk silica values. On the other hand, the AE380 material shows a line peaked at a much lower frequency position, which remains essentially stable up to ∼600 C. On increasing the thermal treatment temperature, also for this material, the line position shifts toward the bulk silica

Thermally Induced Structural Modification of Silica NPs

J. Phys. Chem. C, Vol. 114, No. 33, 2010 **13995**

values. These thermally induced changes resemble those observed for the ω_R line position even if, for the AE380 samples, this latter line starts to change at lower temperatures. This discrepancy could be attributed to the difficulty of the analysis of the IR spectra.

Discussion

Our experimental data clearly show that the fumed silica Raman properties, such as the R-line and the D_1 and D_2 lines, are much more different from those of ordinary bulk silica on decreasing the primary particles' dimension. These findings naturally suggest that these differences, which can be attributed to changes in structural properties of the primary particles, arise from their nanometric dimension. By thermally treating fumed silica, we found that these differences are removed for the R-line, whereas the D_2 line maintains a different amplitude with respect to that of bulk samples. To investigate in detail the uncommon structural properties of fumed silica, we extracted some quantitative information from Raman and IR spectra as a function of the thermal treatment temperatures. In particular, we focused on the modification of the SiOSi mean bond angle, on the concentration of three-membered rings, and on the water content.

The results on the R-line of Raman spectra can be interpreted by a modification of θ by using eq 1. The data reported in Figure 2 show that the θ values in the untreated fumed silica materials are $\theta = 141.4 \pm 0.5$, 142.6 ± 0.2, and 142.8 ± 0.1 for AE380/0, AE150/0, and AEOX50/0, respectively, and they gradually increase by thermal treatments. At a temperature of 1000 C, these values fall within the variability of the SiOSi mean bond angle ($143.6 \leq \theta_{bulk} \leq 144.2$) estimated in bulk silica materials of different commercial origins.

Further support for the change in θ induced by thermal treatments is found by the modification of the IR line position around 2260 cm^{-1} reported in Figure 6. In fact, the observed increase of the peak position indicates an increase of θ.[30−32] For the reasons discussed in the previous paragraph, it is not possible to extract quantitative values of this angle to be compared with those obtained by the R-line position. Nevertheless, the data trend reported in Figures 2 and 6 for Raman and IR spectra, respectively, suggest a similar tendency of the SiOSi mean bond angle to increase by thermal treatment.

It is important to note that, by geometrical construction, the size of a ring and its SiOSi angle are related each other. Simple considerations suggest that, on increasing the ring size, the bond angle should increase too. For example, three- and four-membered rings are characterized by a θ angle of about 129 and 136, respectively.[14] Obviously, it is not possible to attribute to n-membered rings, with $n \geq 5$, a specific bond angle because these rings do not have, in general, a planar or quasi-planar geometrical shape, as for the three- and four-membered rings.[14] Nevertheless, experimental and simulative studies showed that SiOSi mean bond angles from 140 to 150 characterize bulk silica materials. Because it is widely accepted that the network of bulk silica is characterized by a ring distribution centered on six-membered rings, in which 3-, 4-, and $n \geq 9$ membered rings represent the tails, SiOSi mean bond angles from 140 to 150 are to be mainly attributed to five-, six-, and seven-membered rings.[14,33] This ring distribution is flexible and can be modified by external treatments.[13,33] For example, a shift toward smaller-membered rings, corresponding to a decrease of θ, is typically observed in bulk silica materials densified by hydrostatic pressure.[13]

Our untreated samples are characterized by a smaller bond angle than bulk silica, as shown in Figure 2. Furthermore, the
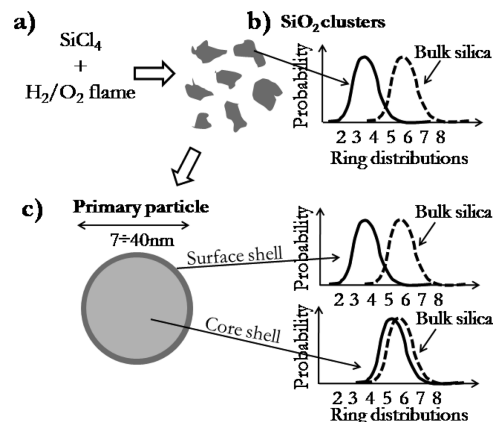

Figure 7. Schematic representation of the formation of fumed silica primary particles: (a) SiCl$_4$ hydrolysis in a H$_2$/O$_2$ flame, (b) formation of small SiO$_2$ clusters, and, finally, (c) the primary particle. The shell-like model of this latter with a core and surface region is shown. The ring distribution of small clusters, bulk silica, and core and surface shells of the primary particle, are qualitatively reported.

D_1 and D_2 Raman lines, assigned to four- and three-membered rings, respectively, are more intense in these materials than in the bulk one (see Figure 1). On the basis of the above-reported discussion, these findings suggest that the ring distribution in fumed silica materials should be slightly shifted toward smaller-membered rings with respect to bulk silica. The angle θ changes induced on fumed silica materials by thermal treatments can be interpreted in terms of modification of the ring distribution. In other words, it could be expected that, when changes are induced on θ, through changes of the R-line, these variations should be reflected on the population of four- and three-membered rings too. However, our results are not in agreement with this scheme. In fact, as shown in Figure 2, the monotonic increase of θ for $T > 500$ C, suggests that the ring distribution in all three fumed silica materials should be gradually shifted toward larger-membered rings. In contrast, as shown in Figure 3, the three-membered ring content increases in the temperature range of 500−800 C.

The above findings show that the population of three-membered rings and of rings with $n > 4$ (contributing to the R-line) have different evolutions by thermal treatments. To interpret these features, it can be supposed that the rings are differently spatially distributed inside the primary particles. In particular, a shell-like structural model of the primary particles of fumed silica can be suggested, as schematically reported in Figure 7, step c. In this scheme, a *surface shell* exists for each particle, characterized by strong structural constraints with a network consisting mainly of small n-membered rings ($n = 3$ and/or 4). In addition, a *core shell* is present showing a network similar to that of the bulk one, but with a ring distribution lightly shifted toward small-membered rings. One can imagine that these different atomic structures of the primary particle are consequences of the strains imposed by the nanometric size of the system. In fact, the surface and near surface are those regions of the particle more affected by the strains resulting from the high radius of curvature.

In support of the shell-like model above presented, it is worth to make reference to some structural properties of silica nanomaterials. In detail, a simple explanation of why the network of a primary particle organizes itself in a shell-like structure can be suggested. Previous theoretical calculations demonstrated that the network of small, free isolated $\{SiO_2\}_n$ clusters ($5 \leq n \leq 20$) are constituted mainly by small-membered

rings, as qualitatively reported in Figure 7, step b.[34−36] This finding was attributed to the fact that the small-membered rings, as compared with bigger ones, are geometrically and energetically favored in forming a stable network of few SiO_2 elements. As shown in the scheme of Figure 7, one can imagine that, in the starting stages of the fumed silica synthesis process ($SiCl_4$ + H_2/O_2 flame), these small clusters represent the early blocks leading to the formation of the primary particles. In this scheme, when these clusters are connected together to build up the primary particle (constituted by many hundreds of these clusters), the original structural constraints pertaining to each cluster forming the core region of the primary particle are partially released thanks to the increase of the degrees of freedom. In other words, the fusion of the primary clusters into larger ones permits the reorganization of the network so that the ring distribution shifts toward larger-membered rings (compare Figure 7, steps b and c). In this respect, it is expected that the structure of the core region becomes similar, but not necessarily identical, to that of bulk silica. At variance, the clusters, connected in proximity of the surface or near surface layer of the particle, remains more constrained. In agreement with this model, simulative studies on SiO_2 nanoparticles showed that the outer layer presents a different atomic network as compared with the inner part.[10,37] It was also found that the thickness of the outer layer is about two reticular steps ($\simeq$2 to 3 Å) and independent of the particles' dimension. In our experimental system, a thickness $\simeq$2 to 3 Å for the exterior layer gives a (surface shell volume)/(particle volume) ratio of about 20, 10, and 4% for particles with 7, 14, and 40 nm diameters, respectively, showing that, depending on the particle size, the surface layer could give a relevant contribution to the overall particle properties. Our experimental results can then be easily interpreted by the shell-like model presented above. In fact, the high intensity of the D_1 and D_2 Raman lines, characterizing all three typologies of untreated fumed silica (see the dotted line in Figure 1), is mainly due to the high content of four- and three-membered rings, respectively, in the surface shell of the primary particles. In particular, as shown in the inset of Figure 3, the D_2 line amplitude of the untreated samples monotonically decreases with increasing the particles' diameter. This result is in agreement with the shell-like model, in which the (surface shell volume)/(particle volume) ratio decreases on increasing the particles' size, if the outer layer is of an almost constant thickness. On the other hand, the evident shift of the Raman R-line position, characterizing all three typologies of untreated fumed silica, is mainly attributable to the residual strains of the core shell network of the particles. As reported in Figure 2, this line is much more shifted toward high frequencies on decreasing the particles' size as a consequence of the fact that the smaller the primary particle is, the more the network of the core shell is strained.

The application of thermal treatments is able to change the overall structural properties of the fumed silica samples: the water content, R-line, and D_1 and D_2 lines are modified. On the basis of the above illustrated shell-like model for the nanoparticles, we interpret these results. First of all, we notice that, as reported in Figure 5, the water content monotonically decreases, starting from the first treatment temperature of 100 C, independent of the material. At variance, the R-line position changes start above 400 C at a value of the temperature that depends on the material (see Figure 2). These findings suggest that the network modifications of the core shell are independent of the drying process. This can also be supported considering the fact that water is adsorbed on the particles' surface, and

therefore, the core shell and the water layer are spatially separated by the surface shell. For this reason, it is not surprising that the shift of the R-line toward lower frequencies is not related to the water release and occurs for $T \geq 400$ C because of thermal relaxation of residual strains in the core shell network. It is important to note that the modification of the R-line starts above 400 C for the AE380 material and above 800 C for the AE150 and AEOX50. This can be attributed to different activation energies for stress removal in the various materials. In detail, AE150 and AEOX50 untreated materials have a similar initial strained network of the core shell with comparable values of θ, and their modifications are triggered at the same temperature. At variance, the AE380 untreated material is characterized by a stronger initial strain (see the lower θ values in Figure 2) that is released starting at lower temperatures.

On the other hand, as shown in Figure 3, the D_2 line increases above 400 C, reaches a maximum at $\simeq$700 C, and successively decreases for higher temperatures with a dependence that looks similar in all fumed silica samples. The increase of this Raman line can be linked to the dehydroxylation process. Indeed, as suggested previously,[9,24,38,39] around $T \simeq 700$ C, the silanol groups on the particles' surface, no longer hydrogen bonded to water molecules, can interact with each other, forming SiOSi bridging bonds ($\equiv$Si−OH HO−Si$\equiv$ → $\equiv$SiOSi$\equiv$ + H_2O).

This hypothesis is somehow corroborated by the decrease of amplitude of the IR bands, related to SiOH groups engaged in H bonding with each other, observed in Figure 4. It is worth noting that the rehydration does not affect this conclusion because hardly any reversible dehydration can be observed above 400 C.[39] The SiOSi bridging bond generation, localized on the particle surfaces, promotes the formation of three-membered rings, and therefore, the D_2 line increases.[9,38] It is important to note that the increase of the D_2 line amplitude around $T = 700$ C is more evident on decreasing the particle diameters (see Figure 3). This finding further corroborates the precursor role of the surface silanol groups in the formation of three-membered rings by thermal treatments. Indeed, the concentration of surface silanol groups (OH/cm^3) is larger on decreasing the particle dimension.[17,40] For temperatures above 700 C, the decrease of the D_2 line amplitude can be interpreted by the occurrence of a different physical process. In this latter, the particle surface, mainly constituted by three-membered rings, is involved in the particle-to-particle bonding, originating the formation of more complex structures and of larger-membered rings, with the ensuing decrease of the D_2 line amplitude. In this respect, it is guessed that the structural modifications involve the single particle below 700 C, whereas at higher temperatures, structural changes are due to the buildup of particle-to-particle linking (sintering effects).

Conclusions

The experimental results presented in this work show that the not treated fumed silica materials are characterized by spectral features significantly different from those of bulk silica. The Raman R-line, the probe of the SiOSi mean bond angle, is shifted toward higher frequencies, and the D_2 line, the probe of three-membered rings, is much more intense in fumed silica. We found that these peculiar properties are more pronounced on decreasing the particles' diameter, suggesting a strong relation with the nanometric nature of fumed silica. The R-line position and the D_2 line amplitude evidence that the ring distribution is characterized in fumed silica by a larger content of small-membered rings than that of bulk silica, showing that the fumed silica network structure is strained. By isochronal

Thermally Induced Structural Modification of Silica NPs

J. Phys. Chem. C, Vol. 114, No. 33, 2010 **13997**

thermal treatments, we found that these Raman features as well as the water content physisorbed on the particles' surface are gradually modified. As a consequence of the fact that the D_2 line modifications are different than those of the R-line, together with the observation that the modifications of this latter line are independent of water content reduction, a shell-like model for the primary particles is suggested. In this model, a surface shell is proposed, consisting mainly of small *n*-membered rings ($n = 3$ and/or 4) with strong structural strains. In addition, a core shell is present, showing a bulklike network with a ring distribution slightly shifted toward small-membered rings. On the basis of this model, the core shell network is strongly modified by thermal treatments, tending toward that typical of bulk silica, whereas the surface shell is less affected and maintains a strained network in the range of the investigated thermal treatments.

References and Notes

(1) Barthel, H.; Heinemann, M.; Stintz, M.; Wessely, B. *Part. Part. Syst. Charact.* **1999**, *16*, 169.

(2) Tan, W. H.; Wang, K. M.; He, X. X.; Zhao, X. J.; Drake, T.; Wang, L.; Bagwe, R. P. *Med. Res. Rev.* **2004**, *24*, 621.

(3) Ruan, W. H.; Huang, X. B.; Wang, X. H.; Rong, M. Z.; Zhang, M. Q. *Macromol. Rapid Commun.* **2006**, *27*, 581.

(4) Abe, I.; Sato, K.; Abe, H.; Naito, M. *Adv. Powder Technol.* **2008**, *19*, 311.

(5) Pratsinis, S. E. *Prog. Energy Combust. Sci.* **1998**, *24*, 197.

(6) Stark, W. J.; Pratsinis, S. E. *Powder Technol.* **2002**, *126*, 103.

(7) Wang, R.; Wunder, S. L. *Langmuir* **2000**, *16*, 5008.

(8) Burneau, A.; Barrès, O.; Gallas, J. P.; Lavalley, J. C. *Langmuir* **1990**, *1364*, 6.

(9) Yamada, T.; Nakajima, M.; Suemoto, T.; Uchino, T. *J. Phys. Chem. C* **2007**, *111*, 12973.

(10) Roder, A.; Kob, W.; Binder, K. *J. Chem. Phys.* **2001**, *114*, 7602.

(11) Uchino, T.; Aboshi, A.; Kohara, S.; Ohishi, Y.; Sakashita, M.; Aoki, K. *J. Non-Cryst. Solids* **2004**, *69*, 155409.

(12) Galeener, F. L. *Solid State Commun.* **1982**, *44*, 1037.

(13) Hehlen, B. *J. Phys.: Condens. Matter* **2010**, *22*, 025401.

(14) Pasquarello, A.; Car, R. *Phys. Rev. Lett.* **1998**, *80*, 5145.

(15) Stesmans, A.; Clémer, K.; Afanas'ev, V. V. *Phys. Rev. B* **2005**, *72*, 155335.

(16) Stesmans, A.; Clémer, K.; Afanas'ev, V. V. *Phys. Rev. B* **2008**, *77*, 094130.

(17) *Basic Characteristics of Aerosil*, 4th ed.; Degussa: Frankfurt, Germany, 2001.

(18) Evonik Industries online catalog, 2010.

(19) Goller, D. D.; Phillips, R. T.; Sayce, I. G. *J. Non-Cryst. Solids* **2009**, *355*, 1747.

(20) Hemley, R. J.; Mao, H. K.; Bell, P. M.; Mysen, B. O. *Phys. Rev. Lett.* **1986**, *57*, 747.

(21) Buscarino, G.; Vaccaro, G.; Agnello, S.; Gelardi, F. M. *J. Non-Cryst. Solids* **2009**, *355*, 1092.

(22) Sen, S. *J. Phys. Chem. B* **2007**, *111*, 9431.

(23) Geissberger, A. E.; Galeener, F. *Phys. Rev. B* **1983**, *28*, 3266.

(24) Zhuravlev, L. T. *Colloids Surf., A* **2000**, *173*, 1.

(25) Gallas, J. P.; Goupil, J. M.; Vimont, J. C.; Lavalley, A.; Gil, B.; Gilson, J. P.; Miserque, M. *Langumir* **2009**, *25*, 5825.

(26) Gallas, J. P.; Lavalley, J. C.; Burneau, A.; Barres, O. *J. Non-Cryst. Solids* **1991**, *7*, 1235.

(27) Morrow, B. A.; McFarlan, A. J. *J. Phys. Chem.* **1992**, *96*, 1395.

(28) Davis, K. M.; Tomozawa, M. *J. Non-Cryst. Solids* **1996**, *201*, 177.

(29) Agarwal, A.; Davis, M. K.; Tomozawa, M. *J. Non-Cryst. Solids* **1995**, *185*, 191.

(30) Galeener, F. L. *Phys. Rev. B* **1979**, *19*, 4292.

(31) Kakiuchida, H.; Saito, K.; Ikushima, A. J. *J. Appl. Phys.* **2003**, *93*, 777.

(32) Tomozawa, M.; Hong, J. W.; Ryu, S. R. *J. Non-cryst. Sol.* **2005**, *351*, 1054.

(33) Giacomazzi, L.; Umari, P.; Pasquarello, A. *Phys. Rev. B* **2009**, *79*, 064202.

(34) Wang, L. S.; Nicholas, J. B.; Dupuis, M.; Wu, H.; Colson, S. D. *Phys. Rev. Lett.* **1997**, *78*, 4450.

(35) Harkless, J. A. W.; Stillinger, D. K.; Stillinger, F. H. *J. Phys. Chem.* **1996**, *100*, 1098.

(36) Xu, C.; Wang, W.; Zhang, W.; Zhuang, J.; Liu, L.; Kong, Q.; Zhao, L.; Long, Y.; Fan, K.; Qian, S.; Li, Y. *J. Phys. Chem. A* **2000**, *104*, 9518.

(37) Schweigert, I. V.; Lehtinen, K. E. J.; Carrier, M. J.; Zachariah, M. R. *Phys. Rev. B* **2002**, *65*, 235410.

(38) Inai, S.; Harao, A.; Nishikawa, H. *J. Non-Cryst. Solids* **2007**, *353*, 510.

(39) Young, G. J. *J. Colloid Sci.* **1958**, *13*, 67.

(40) Zhuravlev, L. T. *Langmuir* **1987**, *3*, 316.

JP103565A